Contents lists available at ScienceDirect

Organic Electronics

journal homepage: www.elsevier.com/locate/orgel

New deep-red heteroleptic iridium complex with 3-hexylthiophene for solution-processed organic light-emitting diodes emitting saturated red and high CRI white colors

Xuejing Liu [a,c], Shumeng Wang [a,c], Bing Yao [a], Baohua Zhang [a,*], Cheuk-Lam Ho [b], Wai-Yeung Wong [b,*], Yanxiang Cheng [a], Zhiyuan Xie [a,*]

[a] State Key Laboratory of Polymer Physics and Chemistry, Changchun Institute of Applied Chemistry, Chinese Academy of Sciences, Changchun 130022, PR China
[b] Institute of Molecular Functional Materials, Department of Chemistry, Institute of Advanced Materials, Hong Kong Baptist University, Waterloo Road, Hong Kong, PR China
[c] University of Chinese Academy of Sciences, Beijing 100049, PR China

ARTICLE INFO

Article history:
Received 17 December 2014
Received in revised form 2 February 2015
Accepted 13 February 2015
Available online 20 February 2015

Keywords:
Solution-processing
Iridium complex
Saturated red emission
White organic light-emitting diode

ABSTRACT

The exploitation of soluble and efficient deep-red phosphorescent emitters is of paramount importance for solution-processed organic light-emitting diodes (OLEDs) applied in both high-quality RGB displays and high color-rendering-index (CRI) solid-state lighting source. In this work, a new deep-red heteroleptic iridium(III) complex, i.e. bis[2,5-di(4-hexylthiophen-2-yl)pyridine][acetylacetonate]iridium(III) [Ir(ht-5ht-py)$_2$(acac)], has been synthesized and successfully used to fabricate solution-processed saturated red and white organic light-emitting diodes (WOLEDs). The long alkyl side-chains of Ir(ht-5ht-py)$_2$(acac) render its excellent solubility in common organic solvents and good compatibility with common host materials. The solution-processed red OLED based on Ir(ht-5ht-py)$_2$(acac) exhibited a decent external quantum efficiency of 8.2% and a power efficiency of 6.5 lm/W, with satisfactory Commission International de L'Eclairage (CIE) coordinates of (0.68, 0.31) for saturated red emission. Furthermore, the prepared multiple-phosphors-doped WOLED with Ir(ht-5ht-py)$_2$(acac) as the red emitter showed an excellent high color rendering index (CRI) value of 89 as well as low color-correlated temperature (CCT) of 2331 K, which can meet the call for physiologically-friendly indoor illumination.

1. Introduction

Solution-processed phosphorescent organic light-emitting diodes (OLEDs) have drawn great attention in the past decades since they hold great potential in large-area and cost-effective manufacturing of flat panel displays and solid-state lighting sources. The efficient phosphorescent emitters that can harvest both singlet and triplet excitons for radiative decay are of paramount importance for achieving high device performance [1–4]. Efficient and solution-processible deep red phosphors and devices are indispensible in various kinds of organic electroluminescent (EL) devices such as red–green–blue (RGB) full color displays and white lighting devices [5]. It not only functions as a primary color for high color quality RGB displays, but also plays an important role in determining the light-emitting efficiency and color quality of white light-emitting devices (WOLEDs) [6–7]. Moreover, the widely used physiologically-friendly "candle-like" white lighting devices also require efficient deep red phosphors to achieve high color rendering index (CRI) and low color correlated temperature (CCT) merits [5]. Although great progress has been achieved in solution-processed red OLEDs by using novel host materials in combination with typical light-red dopants [9–11], deep-red phosphors and devices with CIE-$x \geqslant 0.67$ are still scarce up to now [12,13].

Several saturated red phosphors have been developed previously to improve the light-emitting efficiencies of the solution-processed red OLEDs. For example, Park et al. synthesized an efficient red phosphor [2-(9,9-diethyl-9H-fluoren-2-yl)-4-phenylquinoline]$_2$ iridium(III) picolinic acid *N*-oxide [(FPQ)$_2$Ir(pic-N-O)] and successfully applied it in solution-

* Corresponding authors.
E-mail addresses: bhzhang512@ciac.ac.cn (B. Zhang), rwywong@hkbu.edu.hk (W.-Y. Wong), xiezy_n@ciac.ac.cn (Z. Xie).

http://dx.doi.org/10.1016/j.orgel.2015.02.016
1566-1199/

processed red OLEDs, achieving a luminous efficiency (LE) of 9.9 cd/A, a power efficiency (PE) of 3.9 lm/W and an external quantum efficiency (EQE) of 8.9%, with the CIE coordinates of (0.660, 0.338) [14]. We have reported an efficient saturated deep-red iridium dendrimer containing arylamine units as periphery dendron to realize superior efficiency/color purity trade-offs [10]. The resultant device exhibited a high EQE of 11.65% and a PE of 3.65 lm/W with a CIE coordinate of (0.70, 0.30). In contrast to the dendritic route to develop solution-processible red phosphors [15,16], Chao et al. proposed to modify red tris(1-phenylisoquinoline) iridium [Ir(piq)$_3$] with long side chain to improve its solubility [17], thus facilitating the miscibility with common poly(vinylcarbazole) (PVK) host and leading to a distinct efficiency increase from 0.74 cd/A to ca. 6 cd/A. In spite of these improvements, highly-soluble efficient deep-red phosphors remain scarce and limit the development of high color quality solution-processed red OLEDs and WOLEDs [18–20]. As an example, the CRI values of these WOLEDs were typically less than 80 and thus did not meet the practical requirement for white color lighting.

Here, we synthesized a new solution-processible red heteroleptic iridium(III) complex, i.e. bis[2,5-di(4-hexylthiophen-2-yl)pyridine][acetylacetonate]iridium(III) [Ir(ht-5ht-py)$_2$(acac)], which showed pure red photoluminescence (PL) emission with peak located at 628 nm, corresponding to the CIE coordinates of (0.68, 0.31). The red phosphor [Ir(ht-5ht-py)$_2$(acac)] exhibits good solubility in common organic solvents and excellent miscibility with host in solution process. The corresponding solution-processed red OLED showed a promising EQE of 8% and a PE of 6.5 lm/W. Furthermore, by combining it with a blue phosphorescent iridium(III) [bis(4,6-difluorophenyl)-pyridinato-N,C^2]-picolinate [FIrpic] [21], green phosphorescent G0 [22] and orange phosphorescent dopant containing 5-trifluoromethyl-2-(9,9-diethylfluoren-2-yl)pyridine ligand [Ir(Flpy-CF$_3$)$_3$] [20] to prepare four-color white emissive layer, the resulting WOLEDs show a high CRI of 89 and low CCT of 2331 K, making it a physiologically-friendly white lighting source [8]. This is among a few reports that solution-processed WOLEDs achieve such ideal warm white light emission.

2. Experimental

2.1. General information

All chemicals and reagents were purchased from Aldrich Chemicals Company. The solvents were carefully dried and distilled with appropriate drying agents prior to use. Commercially available reagents were used without further purification unless otherwise stated. The ^{1}H and ^{13}C NMR spectra were recorded with Bruker Advanced 400 MHz NMR spectrometer. Thermal gravimetric analysis (TGA) was performed on Perkin–Elmer-TGA 7 thermal gravimetric analyzer under nitrogen flow at a heating rate of 10 °C/min. MALDI-TOF–TOF was carried out using Bruker autoflex III smart beam mass spectrometer.

2.2. Synthesis of ligand

2,5-Dibromopyridine (2.0 g, 7.55 mmol), 3-hexylthiophene boronic acid (4.0 g, 18.9 mmol) and Pd(PPh$_3$)$_4$ (262.0 mg) were added into a mixture of THF (30 mL) and 2 M Na_2CO_3 (8 mL) under N_2 atmosphere. The reaction mixture was heated to 90 °C for 48 h with stirring. Then the reaction mixture was cooled down to room temperature and extracted with ethyl acetate (EA). The combined organic phase was washed with water. The organic phase was separated and dried over $MgSO_4$. The solvent was removed under reduced pressure and the residue was purified by column chromatography eluting with CH_2Cl_2/hexane. The product was obtained as a white crystalline solid. ^{1}H NMR (400 MHz, $CDCl_3$): δ (ppm) 8.80 (d, J = 1.9 Hz, 1H,Ar), 7.84 (d, J = 6.8 Hz, 1H, Ar), 7.61 (d, J = 8.3 Hz, 1H, Ar), 7.51 (d, J = 4.5 Hz, 1H, Ar), 7.20 (d, J = 1.0 Hz, 1H, Ar), 6.99 (d, J = 11.8 Hz, 1H, Ar), 6.94 (s, 1H, Ar), 2.63 (t, J = 7.7 Hz, 4H, hexyl), 1.72–1.59 (m, 4H, hexyl), 1.42–1.23 (m, 12H, hexyl), 0.90 (dd, J = 7.0, 5.6 Hz, 6H, hexyl). ^{13}C NMR (101 MHz, $CDCl_3$): δ (ppm) 151.31, 146.39, 144.70, 144.47, 143.93, 140.06, 133.26, 128.69, 125.96, 125.19, 122.48, 120.42, 118.55 (Ar), 31.70, 30.65, 30.58, 30.11, 29.01, 22.64, 14.12 (hexyl).

2.3. Preparation of Ir(ht-5ht-py)$_2$(acac)

The phosphorescent iridium complexes were prepared according to the well-established two-step strategy from the cyclometalation of $IrCl_3{\cdot}3H_2O$ with the corresponding organic ligand to form, initially, the μ-chloro-bridged dimer, followed by coordination of the acetylacetone (acac) anion in the presence of Na_2CO_3 [23]. The reaction mixture was extracted with CH_2Cl_2. The combined organic phase was washed with water. The organic phase was separated and dried over $MgSO_4$. The product was purified by silica gel column chromatography with CH_2Cl_2/hexane as an eluent and a dark red solid was obtained. ^{1}H NMR (400 MHz, $CDCl_3$): δ (ppm) 8.49 (d, J = 1.8 Hz, 2H, Ar), 7.68 (dd, J = 8.5, 2.1 Hz, 2H, Ar), 7.36 (d, J = 8.4 Hz, 2H, Ar), 7.04 (t, J = 5.4 Hz, 2H, Ar), 6.81 (s, 2H, Ar), 6.69 (s, 2H, Ar), 5.21 (d, J = 4.1 Hz, 1H, acac), 2.52 (dd, J = 15.2, 7.4 Hz, 4H, alkyl), 1.85–1.66 (m, 9H, alkyl), 1.66–1.44 (m, 12H, alkyl), 1.34–1.09 (m, 28H, alkyl), 1.09–0.93 (m, 11H, alkyl), 0.93–0.72 (m, 19H, alkyl), 0.72–0.60 (m, 8H, alkyl). ^{13}C NMR (101 MHz, $CDCl_3$): δ (ppm) 183.33 (acac), 163.07, 150.44, 146.59, 144.04, 143.56, 138.46, 135.54, 132.75, 124.08, 123.4, 121.51, 118.85, 115.52, 99.86 (Ar), 30.64, 30.48, 29.52, 29.36, 29.09, 28.68, 28.41, 27.95, 27.51, 21.66, 21.56, 13.07, 13.01 (alkyl + acac). Calcd for $C_{55}H_{77}IrN_2O_2S_4$: C, 59.37; H, 6.43; N, 2.52, found: C, 59.33; H, 6.92; N, 2.52. MALDI-TOF–TOF-MS: m/z found 1112.40, calcd 1112.66.

2.4. Photophysical, film morphology and cyclic voltammetry measurements

UV–vis absorption and PL spectra were measured by Perkin–Elmer Lambda 35 UV–vis spectrometer and Perkin–Elmer LS 50B spectrofluorometer, respectively. PL quantum efficiency in solution was measured by the relative method using *fac*-Ir(ppy)$_3$ (Φ_p = 0.40 in toluene) as the standard [24]. AFM measurements were carried out using Veeco Instruments in the tapping mode with a 2 N m^{-1} probe in the atmospheric environment. The sample preparation condition was just the same as device fabrication process. Cyclic voltammetry (CV) experiments were performed on an EG&G 283 (Princeton Applied Research) potentiostat/galvanostat system. All measurements were carried out at room temperature with a conventional three-electrode system consisting of a platinum working electrode, a platinum counter electrode and an Ag/AgCl reference electrode. The supporting electrolyte was 0.1 M tetrabutylammonium perchlorate (n-Bu_4NClO_4). The ferrocene/ferrocenium (Fc/Fc^+) couple was used as the internal standard. Emission lifetime was obtained by single exponential fit of emission decay curve measured for dilute sample solution (10^{-5} M), which was recorded on a system equipped with a Quanty-ray DCR-2 pulsed Nd:YAG laser.

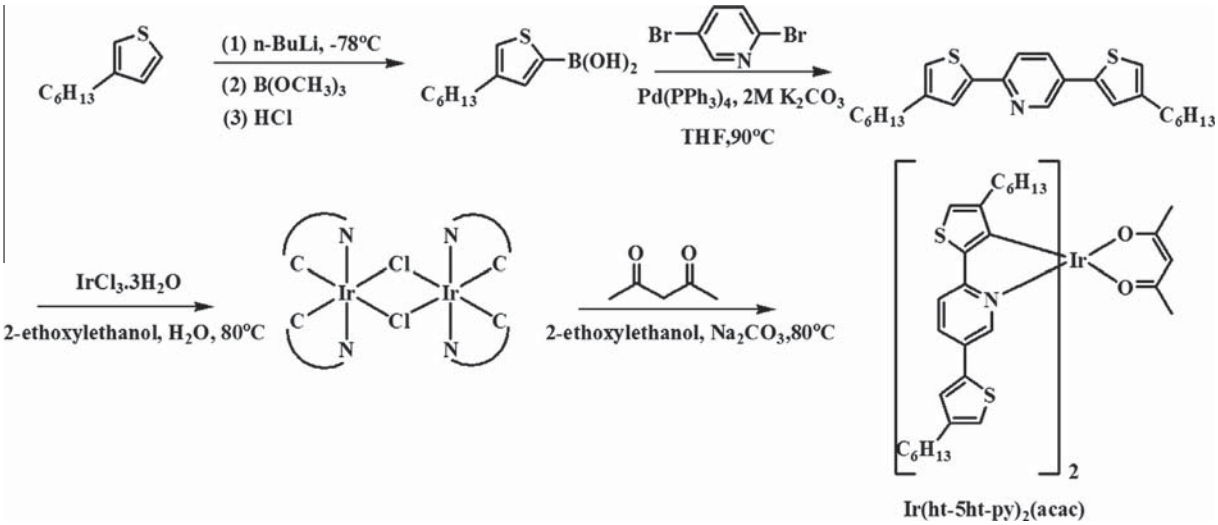

Scheme 1. The synthetic route of the ligand and its iridium complex.

2.5. Material information

4,4′,4″-Tris(*N*-carbazolyl)-triphenylamine (TCTA) and poly-(ethylenedioxythiophene): poly(styrenesulfonate) (PEDOT:PSS) (Baytron P Al 4083) were purchased from Luminance Technology Corp. and H.C. Starck Clevios GmbH, respectively, and used as received. The materials including FIrpic, G0, Ir(Flpy-CF_3)$_3$ and 2,7-bis(diphenylphosphoryl)-9,9′-spirobi[fluorene] (SPPO13) were synthesized according to the literature method [20–22,25].

2.6. Device fabrication and testing

The solution-processed red and white OLEDs were fabricated with a structure of ITO/PEDOT:PSS (50 nm)/emissive layer (40 nm)/SPPO13 (65 nm)/LiF (1 nm)/Al (100 nm). The ITO substrates were pre-cleaned with routine procedure and treated by UV–ozone for 30 min. A layer of PEDOT:PSS was deposited on the ITO substrate via spin-coating to form a hole injection layer. The PEDOT:PSS-coated substrates were baked in oven at 120 °C for 45 min. The emissive layer (EML) consisting of TCTA doped with Ir(ht-5ht-py)$_2$(acac) (2, 4 or 6 wt.%) was spin-coated from fresh chlorobenzene solution. As for the white EML, the ratio of TCTA to FIrpic, G0 and Ir(Flpy-CF_3)$_3$ was fixed at 100:20:1.0:0.8 (w/w/

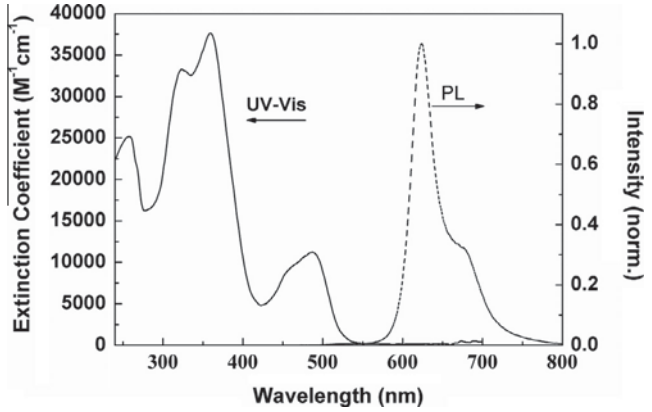

Fig. 1. Absorption (left) and PL spectra (right) of red phosphor Ir(ht-5ht-py)$_2$(acac) in CH_2Cl_2 solution with a concentration of 10^{-5} M.

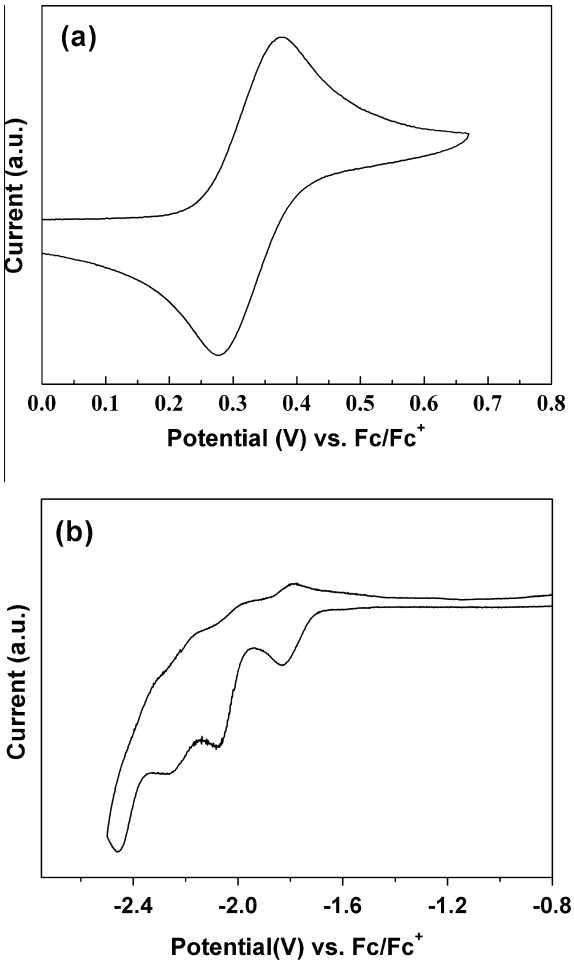

Fig. 2. Cyclic voltammograms of Ir(ht-5ht-py)$_2$(acac).

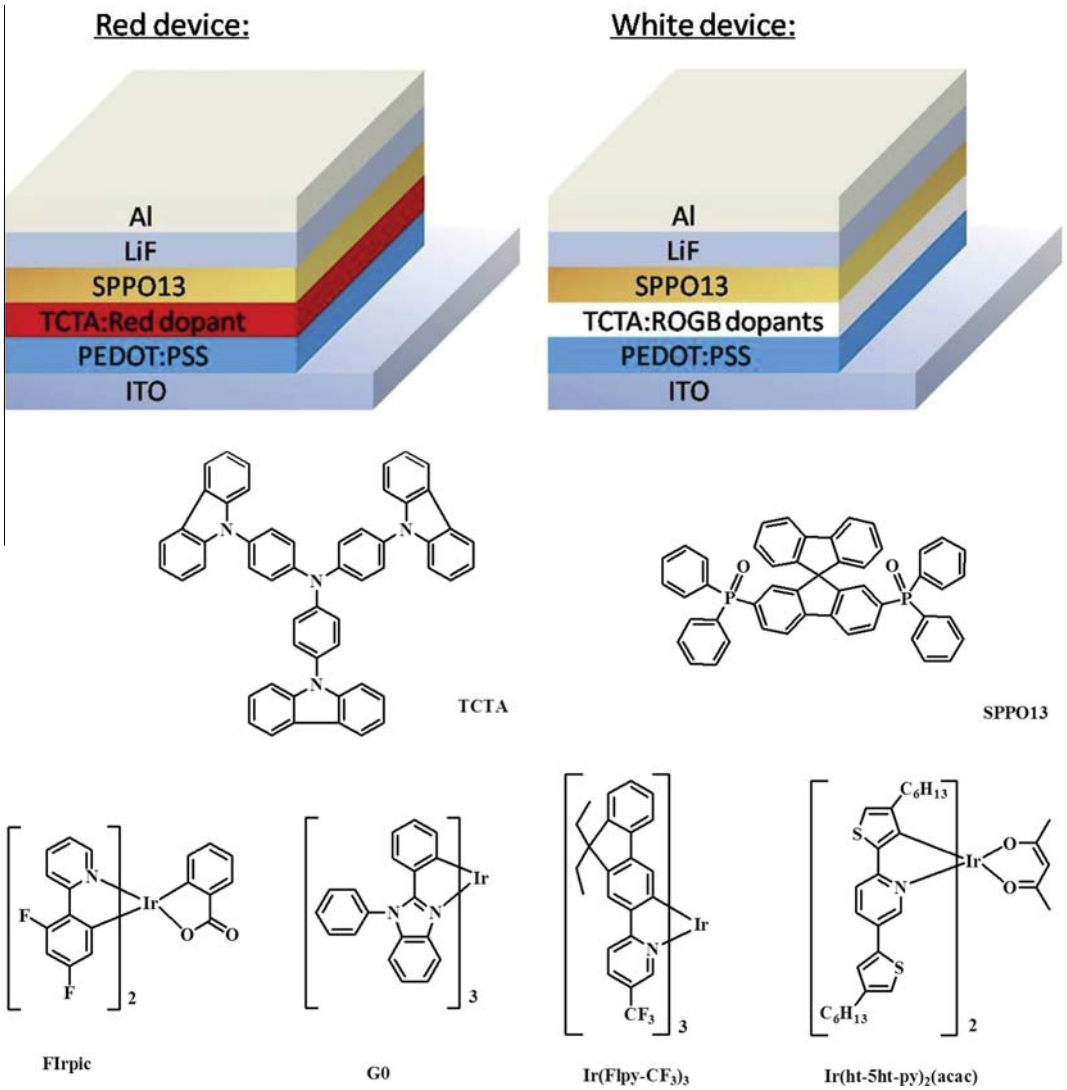

Fig. 3. The device configurations and chemical structures of the materials used.

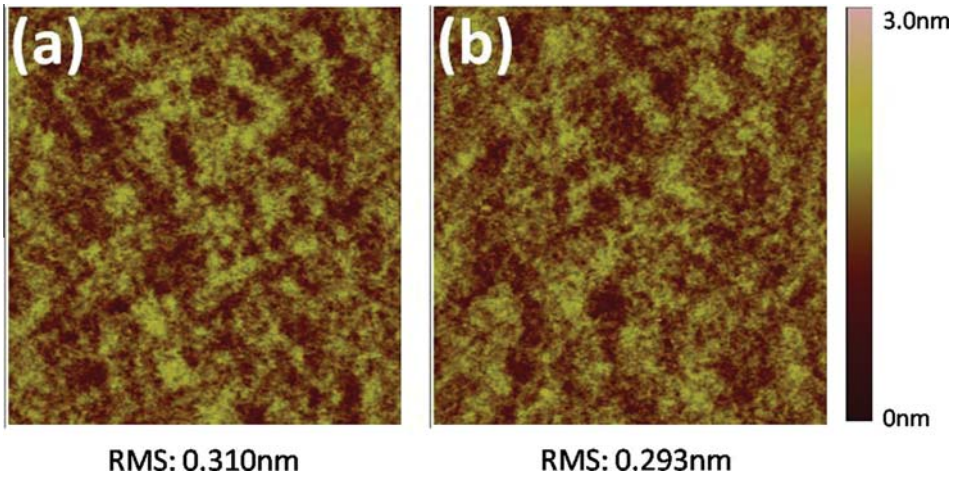

Fig. 4. The topography images of (a) TCTA and (b) TCTA: Ir(ht-5ht-py)$_2$(acac) (4 wt.%) film measured by AFM.

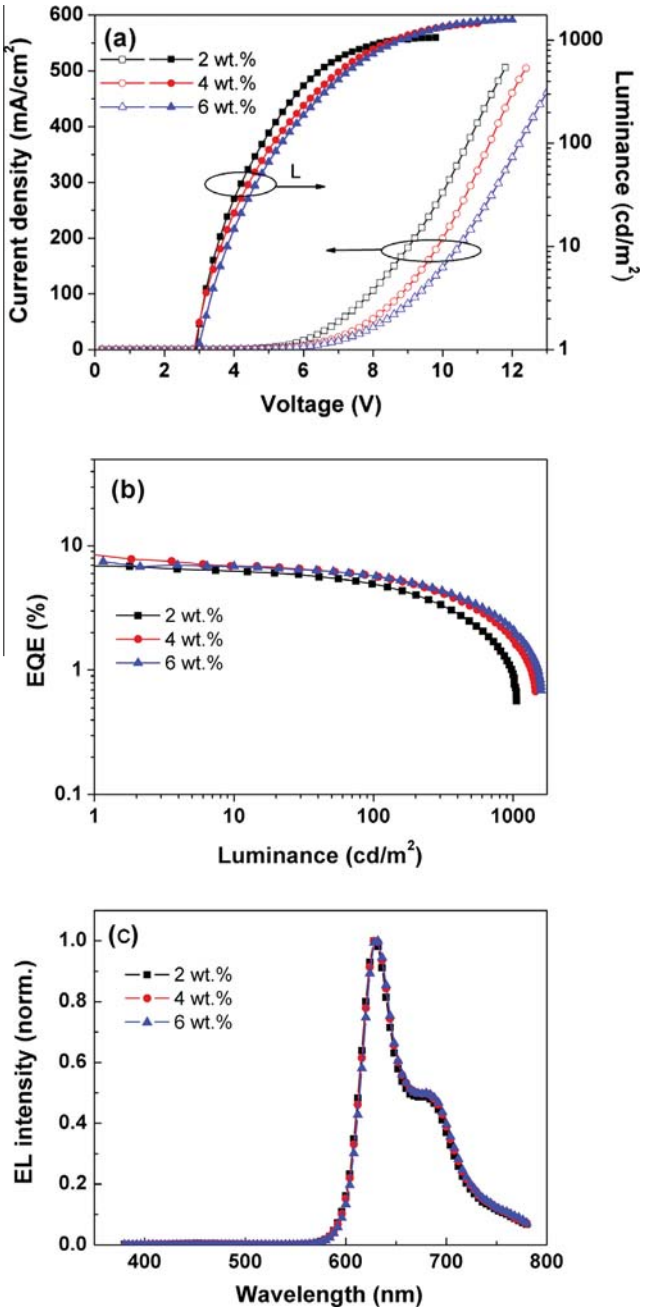

Fig. 5. Device performance of the red device based on Ir(ht-5ht-py)$_2$(acac) with different doping ratios: (a) *J*–*V*–*L* characteristics; (b) EQE–L curve; and (c) EL spectra. (For interpretation of the references to colour in this figure legend, the reader is referred to the web version of this article.)

w/w), and emission spectra were solely tuned by changing the concentration of Ir(ht-5ht-py)$_2$(acac). A device structure of SPPO13 (65 nm)/LiF (1 nm)/Al (100 nm) was thermally deposited in sequence in a vacuum chamber at a base pressure of less than 4×10^{-4} Pa. The current density (*J*)–luminance (*L*)–voltage (*V*) characteristics were measured by a Keithley source measurement unit (Keithley 2400 and Keithley 2000) with a calibrated silicon photodiode. The EL spectra of the devices were measured by SpectraScan PR650 spectrophotometer. All measurements were carried out at room temperature under ambient conditions. EQEs of the devices were calculated from the luminance, current density and EL spectrum, assuming a Lambertian distribution.

3. Results and discussion

The synthetic route of the ligand and Ir(ht-5ht-py)$_2$(acac) is shown in Scheme 1. The key ligand precursor is the 3-hexylthiophene boronic acid, synthesized from 3-hexylthiophene, *n*-butyl lithium and trimethyl borate in dry THF in an ice-acetone bath. The ligand was synthesized by the palladium-catalyzed Suzuki cross-coupling of 2,5-dibromopyridine with 3-hexanethiopheno boronic acid. Then $IrCl_3 \cdot nH_2O$ reacted with an excess of the ligand to give the chloride-bridged iridium dimer. The dimer could be readily cleaved to the monomeric complex by replacing the bridging chlorides with acetylacetonate anion (acac) in the presence of sodium carbonate [23].

The thermal property of Ir(ht-5ht-py)$_2$(acac) was characterized by TGA under nitrogen. As measured, the 5% weight-reduction temperature is as high as 309 °C, indicating that the red phosphor is thermally very stable. The absorption and PL spectra of Ir(ht-5ht-py)$_2$(acac) in dichloromethane solution are shown in Fig. 1. As depicted, the red Ir complex exhibits strong absorption bands in the 200–425 nm region that are assigned to ligand-centered $^1\pi-\pi^*$ transition. The absorption bands with lower extinction coefficients in the range of 425–540 nm are ascribed to singlet and triplet metal to ligand charge-transfer (^{1}MLCT and ^{3}MLCT) states induced by the strong spin–orbital coupling [13,26,27]. The PL emission of Ir(ht-5ht-py)$_2$(acac) is centered at 628 nm in the deep-red region. Ir(ht-5ht-py)$_2$(acac) complex shows a decay lifetime as short as 0.95 μs in degassed toluene solution. As reported, the short phosphorescent lifetime is advantageous to lower the possible triplet–triplet annihilation in OLEDs [28–30]. The electrochemical characteristics of the red complex shown in Fig. 2 show that there is a reversible one-electron oxidation in CH_2Cl_2 solution. Since the ligand does not display oxidation waves in this potential region, the low positive oxidation potential is attributed to the Ir centered oxidation [31]. Besides, under the condition of oxygen removal, four reduction waves in DMF solution were observed. Among them, the first reduction potential was used to determine the LUMO energy level. The calculated HOMO and LUMO levels of Ir(ht-5ht-py)$_2$(acac) are −5.05 and −3.09 eV, respectively. Besides, the measured PL quantum efficiency of Ir(ht-5ht-py)2(acac) is 0.121 in degassed toluene relative to fac-Ir(ppy)$_3$(Φ_p = 0.40) as a standard.

Both red and white OLEDs based on the red phosphor Ir(ht-5ht-py)$_2$(acac) were investigated and the corresponding device configurations are shown in Fig. 3. The red OLEDs have a configuration of ITO/PEDOT:PSS (50 nm)/TCTA: Ir(ht-5ht-py)$_2$(acac)(*x* wt.%, ca. 40 nm)/ SPPO13 (65 nm)/LiF (1 nm)/Al (100 nm). Long side chain in Ir(ht-5ht-py)$_2$(acac) renders it excellent solubility in aromatic solvent (e.g. >30 mg/mL in chlorobenzene) and good miscibility with the TCTA host to form homogeneous EML. The topography images of TCTA:Ir(ht-5ht-py)$_2$(acac) film measured by AFM are homogenous (seen in Fig 4.). The root mean square (RMS) roughness of pure TCTA film and the Ir(ht-5ht-py)$_2$(acac)-doped EML is similar, (0.310 and 0.293 nm, respectively), further indicating the good miscibility between Ir(ht-5ht-py)$_2$(acac) and the TCTA host. The EL characteristics of the red OLEDs, including *J*–*V*–*L* curves, EQE and EL spectra, are displayed in Fig. 5 and some key performance parameters of the red OLEDs are summarized in Table 1. It can be seen in Fig. 5(a) that the current density is gradually decreased with increasing doping concentration of Ir(ht-5ht-py)$_2$(acac) from 2 wt.% to 6 wt.%, inferring that charge trapping effect is

Table 1
Performance of the red OLEDs A-C.

Device	Phosphor dopant	$V_{turn\text{-}on}$ (V)	Luminance (cd/m^2)[a]	η_L (cd/A)[a]	η_p (lm/W)[a]	EQE (%)	λ_{max} (nm)[b]
A	2 wt.%	2.8	1022	4.7	5.3	6.9	628 (0.68, 0.31)
B	4 wt.%	3.0	1548	5.8	6.5	8.2	628 (0.68, 0.31)
C	6 wt.%	3.0	1582	4.9	5.2	7.5	628 (0.69, 0.31)

[a] Maximum values of the devices.
[b] Data were collected at 7 V; CIE coordinates shown in parentheses.

possibly involved for the EL emission in addition to the energy transfer process from TCTA to Ir(ht-5ht-py)$_2$(acac). It is reasonable since both HOMO and LUMO level positions of Ir(ht-5ht-py)$_2$(acac) are located within the HOMO of −5.83 eV and LUMO of −2.43 eV of TCTA host [32]. The turn-on voltage of red OLEDs is as low as 3.0 V, irrespective of the Ir(ht-5ht-py)$_2$(acac) doping ratio. Such driving voltages are actually low compared to the earlier reported red OLEDs with similar device structures [17,33–35]. In view of the similar HOMO/LUMO positions of the red phosphors used, such low driving voltages might be attributed to the homogeneous morphology of the EML. As reported, the homogeneous morphology of the solution-processed EML is beneficial for lowering the driving voltages of the devices [36]. The EQE curves of the red devices A–C are shown in Fig. 5(b). At a doping concentration of 4 wt.% for Ir(ht-5ht-py)$_2$(acac), the resultant red-emitting device achieved a maximum EQE of 8% and a PE of 6.5 lm/W with saturated red CIE coordinates of (0.68, 0.31), which are among the highest efficiencies ever reported for solution-processed deep-red OLEDs [13,17,34,35]. Fig. 5(c) shows that the devices A–C exhibit the same red color emission from Ir(ht-5ht-py)$_2$(acac) with doping concentrations of 2–6 wt.%.

Solution-processed all-phosphor-doped WOLEDs were further prepared by using red phosphor Ir(ht-5ht-py)$_2$(acac). Solution-processed WOLEDs have drawn great research interest in recent years due to their unique advantages, such as simple device structures and low-cost solution-processing, *etc*. The solution-processed WOLEDs have received large progress with EQE surpassing 25% and PE approaching 50 lm/W [37]. However, low CRI value is a common issue encountered for these WOLEDs due to the lack of suitable deep-red phosphor [19]. Here, four-color phosphorescent WOLEDs were prepared with a structure of ITO/PEDOT:PSS (50 nm)/TCTA:FIrpic:G0:Ir(Flpy-CF_3)$_3$:Ir(ht-5ht-py)$_2$(acac) (100:20:1:0.8:*x*, ca. 40 nm)/SPPO13 (65 nm)/LiF(1 nm)/Al (100 nm) as shown in Fig. 3. The EL performance of the WOLEDs, including *J–V–L* curves, luminous efficiencies and EL spectra, are displayed in Fig. 6 and some key parameters of the WOLEDs are summarized in Table 2. We can see that, with gradually increasing the concentration of Ir(ht-5ht-py)$_2$(acac) from 0.4 to 1.2 wt.%, the CRI values of the resultant WOLEDs are distinctly enhanced from 65 to 89, along with gradually decreasing CCT from 3320 K to 2331 K. Such high CRI value is sufficient for general white lighting and was rarely reported previously for solution-processed all-phosphor-doped white-emitting devices. Very recently, Jou et al. [8] firstly reported red-dominant "candle-like" thermal-evaporated WOLEDs from the physiologically-friendly point of view. The solution-processed WOLED device F can meet the requirements. As shown in Fig. 6(c), with increasing concentration of Ir(ht-5ht-py)$_2$(acac), the red contribution relative to the blue, green and orange emissions is enhanced and the total emission gradually approaches the ideal "candle-like" warm white emission. As for the emission mechanisms, on the one hand, direct exciton generation on Ir(ht-5ht-py)$_2$(acac) dopant should play the role on the gradually enhanced red

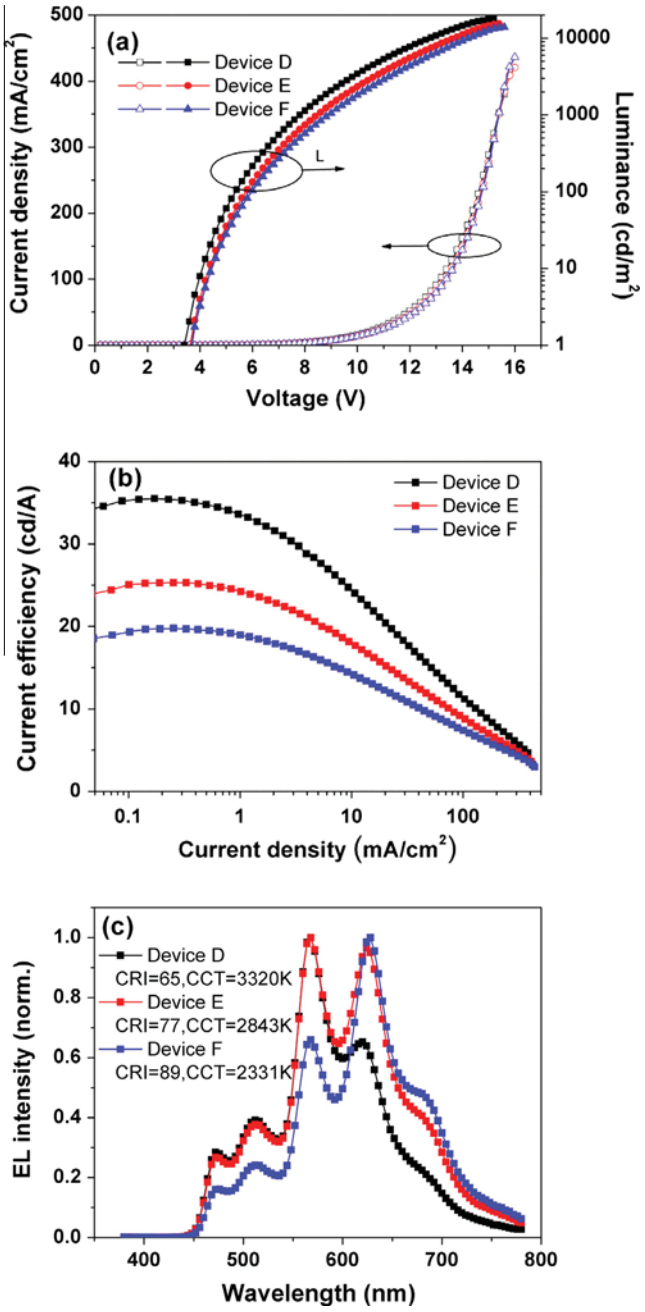

Fig. 6. Device performance of the ROGB four-color WOLEDs with red Ir(ht-5ht-py)$_2$(acac) loading content from 0.4 wt.% to 1.2 wt.% (a) *J–V–L* characteristics; (b) EQE–J curve; and (c) EL spectra at a luminance of ca. 1000 cd/m^2. (For interpretation of the references to colour in this figure legend, the reader is referred to the web version of this article.)

Table 2
Performance of the BGOR four-color WOLEDs.

Device	B:G:O:R (w/w/w/w)	$V_{turn-on}$ (V)	L_{max} (mA/cm^2)	η_L (cd/A)[a]	η_p (lm/W)[a]	EQE (%)[a]	CRI[b]	CCT (K)[b]	CIE coordinates (x,y)[b]
D	20:1:0.8:0.4	3.4	18,013	35.5	26.6	14.1	65	3320	(0.44, 0.47)
E	20:1:0.8:0.8	3.6	15,344	25.3	17.3	11.8	77	2843	(0.47, 0.45)
F	20:1:0.8:1.2	3.6	13,882	19.8	13.2	11.3	89	2331	(0.51, 0.43)

[a] Maximum values of the devices.
[b] Data were collected at a luminance of ca. 1000 cd/m^2.

emission component of the white spectra as increasing the concentration of Ir(ht-5ht-py)$_2$(acac) from device D to F. On the other hand, the simultaneously lowered emission from blue, green and orange parts indicates that Förster/Dexter energy transfer from TCTA and/or high content FIrpic to Ir(ht-5ht-py)$_2$(acac) dopant should also be taken into account. The J–V curves shown in Fig. 6(a) do not exhibit obvious changes with increasing the Ir(ht-5ht-py)$_2$(acac) content from 0.4 to 1.2 wt.%, which is due to distinctly low absolute concentration of Ir(ht-5ht-py)$_2$(acac) in these devices. The device D achieved the highest luminous efficiency (LE) of 35.5 cd/A. However, its CRI is merely 65 due to the weak red emission. The WOLED device F improved the CRI to 89 while the peak LE, PE and EQE decreased to 19.8 cd/A, 13.2 lm/W and 11.3%, respectively. Compared to the earlier reports with low CRI level [18–20,37] (less than 70 in typical), such high CRI value is very excellent and suitable for warm white light from the physiologically-friendly point of view [8]. As for the declined device efficiencies, the relatively low PL quantum efficiency of Ir(ht-5ht-py)$_2$(acac) with respect to FIrpic, G0 and Ir(Flpy-CF$_3$)$_3$ should be the main reason. Although the design and synthesis of efficient red emitters is intrinsically more difficult according to the energy-gap law [38], efforts should be continued to pursue deep-red phosphors of high PL quantum efficiency for further development of solution-processed deep-red and white OLEDs.

4. Conclusions

In summary, a solution-processible deep-red heteroleptic iridium complex Ir(ht-5ht-py)$_2$(acac) was synthesized and successfully used to fabricate solution- processed red and white OLEDs. This iridium complex emits pure red light with emission peak located at 628 nm corresponding to the CIE coordinates of (0.68, 0.31). The introduction of two hexyl side chains on the ligand renders the red phosphor Ir(ht-5ht-py)$_2$(acac) high solubility in common organic solvents and good miscibility with host material to form a homogeneous emissive layer, which is crucial to achieve high-performance solution-processed OLEDs. With a simple device structure, the solution-processed red OLEDs based on Ir(ht-5ht-py)$_2$(acac) achieve an external quantum efficiency of 8% and a power efficiency of 6.5 lm/W. The four-color all-phosphor-doped WOLEDs with Ir(ht-5ht-py)$_2$(acac) as deep red phosphor exhibits a respectable CRI of 89 and a low CCT of 2331 K, which is a requirement for a red-dominant warm white light from the physiologically-friendly point of view.

Acknowledgements

Z.-Y.X and B.-H.Z acknowledge financial support from the National Basic Research Program of China (973 Project, Grant 2014CB643504) and the NSFC of China (Nos. 51103147, 51473162, 51325303). The financial support of the Strategic Priority Research Program of the Chinese Academy of Sciences (XDB12030200) is also acknowledged. W.-Y.W. thanks Hong Kong Research Grants Council (HKBU203312), Areas of Excellence Scheme of HKSAR (AoE/P-03/08) and Hong Kong Baptist University (FRG2/13-14/083) for financial support. The project was also supported by Open Research Fund of State Key Laboratory of Polymer Physics and Chemistry, Changchun Institute of Applied Chemistry, Chinese Academy of Sciences.

References

[1] S. Reineke, M. Thomschke, B. Lüssem, K. Leo, Rev. Mod. Phys. 85 (2013) 1245.
[2] M. Zhu, J. Zou, S. Hu, C. Li, C. Yang, H. Wu, J. Qin, Y. Cao, J. Mater. Chem. 22 (2012) 361.
[3] X. Cao, J. Miao, M. Zhu, C. Zhong, C. Yang, H. Wu, J. Qin, Y. Cao, Chem. Mater. 27 (2015) 96–104.
[4] C. Fan, C. Yang, Chem. Soc. Rev. 43 (2014) 6439.
[5] K.S. Yook, J.Y. Lee, Adv. Mater. 26 (2014) 4218.
[6] K.T. Kamtekar, A.P. Monkman, M.R. Bryce, Adv. Mater. 22 (2010) 572.
[7] H. Wu, L. Ying, W. Yang, Y. Cao, Chem. Soc. Rev. 38 (2009) 3391.
[8] J.-H. Jou, C.-Y. Hsieh, J.-R. Tseng, S.-H. Peng, Y.-C. Jou, J.H. Hong, S.-M. Shen, M.-C. Tang, P.-C. Chen, C.-H. Lin, Adv. Funct. Mater. 23 (2013) 2750.
[9] Y. Tao, Q. Wang, C. Yang, K. Zhang, Q. Wang, T. Zou, J. Qin, D. Ma, J. Mater. Chem. 18 (2008) 4091.
[10] K.H. Kim, J.Y. Lee, T.J. Park, W.S. Jeon, G.P. Kennedy, J.H. Kwon, Synth. Met. 160 (2010) 631.
[11] C. Fan, J. Miao, B. Jiang, C. Yang, H. Wu, J. Qin, Y. Cao, Org. Electron. 14 (2013) 3392.
[12] C.H. Fan, P. Sun, T.H. Su, C.H. Cheng, Adv. Mater. 23 (2011) 2981.
[13] G.-J. Zhou, W.-Y. Wong, B. Yao, Z. Xie, L. Wang, Angew. Chem. Int. Ed. 46 (2007) 1149.
[14] J. Park, J.S. Park, Y.G. Park, J.Y. Lee, J.W. Kang, J. Liu, L.M. Dai, S.H. Jin, Org. Electron. 14 (2013) 2114.
[15] J. Ding, J. Lü, Y. Cheng, Z. Xie, L. Wang, X. Jing, F. Wang, Adv. Funct. Mater. 18 (2008) 2754.
[16] M. Zhu, Y. Li, J. Miao, B. Jiang, C. Yang, H. Wu, J. Qin, Y. Cao, Org. Electron. 15 (2014) 1598.
[17] Y.-C. Chao, S.-Y. Huang, C.-Y. Chen, Y.-F. Chang, H.-F. Meng, F.-W. Yen, I.F. Lin, H.-W. Zan, S.-F. Horng, Synth. Met. 161 (2011) 148.
[18] F. Huang, P.-I. Shih, C.-F. Shu, Y. Chi, A.K.Y. Jen, Adv. Mater. 21 (2009) 361.
[19] J. Zou, H. Wu, C.S. Lam, C. Wang, J. Zhu, C. Zhong, S. Hu, C.L. Ho, G.J. Zhou, W.C. Choy, J. Peng, Y. Cao, W.Y. Wong, Adv. Mater. 23 (2011) 2976.
[20] B. Zhang, G. Tan, C.S. Lam, B. Yao, C.L. Ho, L. Liu, Z. Xie, W.-Y. Wong, J. Ding, L. Wang, Adv. Mater. 24 (2012) 1873.
[21] S. Tokito, T. Iijima, Y. Suzuri, H. Kita, T. Tsuzuki, F. Sato, Appl. Phys. Lett. 83 (2003) 569.
[22] J. Ding, J. Gao, Y. Cheng, Z. Xie, L. Wang, D. Ma, X. Jing, F. Wang, Adv. Funct. Mater. 16 (2006) 575.
[23] S. Chen, G. Tan, W.-Y. Wong, H.-S. Kwok, Adv. Funct. Mater. 21 (2011) 3785.
[24] K.A. King, P.J. Spellane, R.J. Watts, J. Am. Chem. Soc. 107 (1985) 1431.
[25] S.E. Jang, C.W. Joo, J.Y. Lee, Thin Solid Films 519 (2010) 906.
[26] A. Tsuboyama, H. Iwawaki, M. Furugori, T. Mukaide, J. Kamatani, S. Igawa, T. Moriyama, S. Miura, T. Takiguchi, S. Okada, M. Hoshino, K. Ueno, J. Am. Chem. Soc. 125 (2003) 12971.
[27] S. Lamansky, P. Djurovich, D. Murphy, F. Abdel-Razzaq, H.E. Lee, C. Adachi, P.E. Burrows, S.R. Forrest, M.E. Thompson, J. Am. Chem. Soc. 123 (2001) 4304.
[28] C. Adachi, M.A. Baldo, S.R. Forrest, S. Lamansky, M.E. Thompson, R.C. Kwong, Appl. Phys. Lett. 78 (2001) 1622.
[29] G.-J. Zhou, W.-Y. Wong, B. Yao, Z. Xie, L. Wang, J. Mater. Chem. 18 (2008) 1799.
[30] E.B. Namdas, A. Ruseckas, I.D.W. Samuel, S.-C. Lo, P.L. Burn, Appl. Phys. Lett. 86 (2005) 091104.
[31] M. Lepeltier, F. Dumur, G. Wantz, N. Vila, I. Mbomekallé, D. Bertin, D. Gigmes, C.R. Mayer, J. Lumin. 143 (2013) 145.
[32] Y.-S. Park, K.-H. Kim, J.-J. Kim, Appl. Phys. Lett. 102 (2013) 153306.
[33] X. Wang, S. Wang, Z. Ma, J. Ding, L. Wang, X. Jing, F. Wang, Adv. Funct. Mater. 24 (2014) 3413.

[34] J. Chen, C. Shi, Q. Fu, F. Zhao, Y. Hu, Y. Feng, D. Ma, J. Mater. Chem. 22 (2012) 5164.
[35] C.L. Ho, W.Y. Wong, Z.Q. Gao, C.H. Chen, K.W. Cheah, B. Yao, Z.Y. Xie, Q. Wang, D.G. Ma, L.A. Wang, X.M. Yu, H.S. Kwok, Z.Y. Lin, Adv. Funct. Mater. 18 (2008) 319.
[36] Y.Y. Noh, C.L. Lee, J.J. Kim, K. Yase, J. Chem. Phys. 118 (2003) 2853.
[37] B.H. Zhang, L.H. Liu, Z.Y. Xie, Isr. J. Chem. 54 (2014) 897.
[38] J.V. Caspar, E.M. Kober, B.P. Sullivan, T.J. Meyer, J. Am. Chem. Soc. 104 (1982) 630.